



## Research paper

# Efficacy of adeno-associated virus gene therapy in a MNGIE murine model enhanced by chronic exposure to nucleosides



Ferran Vila-Julià<sup>a</sup>, Raquel Cabrera-Pérez<sup>a</sup>, Yolanda Cámara<sup>a</sup>, Miguel Molina-Berenguer<sup>a</sup>, Silvia Lope-Piedrafita<sup>b,c</sup>, Michio Hirano<sup>d</sup>, Federico Mingozzi<sup>e</sup>, Javier Torres-Torronteras<sup>a,\*</sup>, Ramon Martí<sup>a,\*</sup>

<sup>a</sup> Research Group on Neuromuscular and Mitochondrial Diseases, Vall d'Hebron Research Institute, Universitat Autònoma de Barcelona, and Biomedical Network Research Centre on Rare Diseases (CIBERER), Instituto de Salud Carlos III, Barcelona, Catalonia, Spain

<sup>b</sup> Servei de Resonància Magnètica Nuclear, Universitat Autònoma de Barcelona, Cerdanyola del Vallès, Catalonia, Spain

<sup>c</sup> Centro de Investigación Biomédica en Red en Bioingeniería, Biomateriales y Nanomedicina (CIBER-BBN), Cerdanyola del Vallès, Catalonia, Spain

<sup>d</sup> Department of Neurology, H. Houston Merritt Neuromuscular Research Center, Columbia University Irving Medical Center, New York, NY, United States

<sup>e</sup> Spark Therapeutics, Philadelphia, PA 19104, United States

## ARTICLE INFO

## Article History:

Received 17 September 2020

Revised 5 November 2020

Accepted 5 November 2020

Available online xxx

## Keywords:

MNGIE

Gene therapy

Nucleosides

Mitochondrial disease

Thymidine phosphorylase

## ABSTRACT

**Background:** Preclinical studies have shown that gene therapy is a feasible approach to treat mitochondrial neurogastrointestinal encephalomyopathy (MNGIE). However, the genetic murine model of the disease (Tymp/Upp1 double knockout, dKO) has a limited functional phenotype beyond the metabolic imbalances, and so the studies showing efficacy of gene therapy have relied almost exclusively on demonstrating correction of the biochemical phenotype. Chronic oral administration of thymidine (dThd) and deoxyuridine (dUrd) to dKO mice deteriorates the phenotype of the animals, providing a better model to test therapy approaches.

**Methods:** dKO mice were treated with both dThd and dUrd in drinking water from weaning until the end of the study. At 8 - 11 weeks of age, mice were treated with several doses of adeno-associated virus (AAV) serotype 8 vector carrying the human *TYMP* coding sequence under the control of different liver-specific promoters (TBG, AAT, or HLP). The biochemical profile and functional phenotype were studied over the life of the animals.

**Findings:** Nucleoside exposure resulted in 30-fold higher plasma nucleoside levels in dKO mice compared with non-exposed wild type mice. AAV-treatment provided elevated TP activity in liver and lowered systemic nucleoside levels in exposed dKO mice. Exposed dKO mice had enlarged brain ventricles (assessed by magnetic resonance imaging) and motor impairment (rotarod test); both were prevented by AAV treatment. Among all promoters tested, AAT showed the best efficacy.

**Interpretation:** Our results show that AAV-mediated gene therapy restores the biochemical homeostasis in the murine model of MNGIE and, for the first time, demonstrate that this treatment improves the functional phenotype.

**Funding:** This work was funded in part by the Spanish Instituto de Salud Carlos III, and the Generalitat de Catalunya. The disclosed funders had no role in study design, data collection and analysis, decision to publish, or preparation of the manuscript.

© 2020 The Authors. Published by Elsevier B.V. This is an open access article under the CC BY-NC-ND license (<http://creativecommons.org/licenses/by-nc-nd/4.0/>)

## 1. Introduction

Mitochondrial neurogastrointestinal encephalomyopathy (MNGIE) is caused by mutations in the nuclear gene *TYMP* [1], which lead to a deficiency of thymidine phosphorylase (TP) activity and

systemic accumulation of its substrates, the nucleosides thymidine (dThd) and deoxyuridine (dUrd) [2,3]. dThd and dUrd accumulation causes an imbalance in the mitochondrial deoxyribonucleoside triphosphate (dNTP) pool that interferes with mitochondrial DNA (mtDNA) replication, thereby inducing mtDNA depletion, multiple deletions, and point mutations [4-8].

The main clinical features of MNGIE are progressive gastrointestinal dysmotility, cachexia, ptosis, ophthalmoplegia or ophthalmoparesis, demyelinating peripheral neuropathy, symmetrical distal

\* Corresponding authors.

E-mail addresses: [javier.torres@vhir.org](mailto:javier.torres@vhir.org) (J. Torres-Torronteras), [ramon.marti@vhir.org](mailto:ramon.marti@vhir.org) (R. Martí).

## Research in context

### Evidence before this study

Mitochondrial neurogastrointestinal encephalomyopathy (MNGIE) is a fatal metabolic disease caused by mutations in the nuclear gene *TYMP* that encodes thymidine phosphorylase. In patients, thymidine phosphorylase dysfunction causes accumulation of the nucleosides thymidine and deoxyuridine, which interferes with mitochondrial DNA replication. Hence, all therapy approaches for MNGIE are addressed to reach permanent reduction of these toxic metabolites. Over the last years, several preclinical studies have demonstrated that gene therapy is a feasible strategy for this disorder. Transduction of hematopoietic progenitors with the correct version of the gene using lentiviral vectors, or the liver, using an adeno-associated virus (AAV) vector, resulted in effective and sustained restoration of nucleoside homeostasis in the *Tymp/Upp1* double knock out murine model of this disorder. However, this animal model does not recapitulate the clinical manifestations of the disease, and all evidence so far collected supporting gene therapy for MNGIE relies almost exclusively on demonstrating correction of the biochemical phenotype in mice.

### Added value of this study

Previous studies demonstrated that challenging the MNGIE mouse model with a chronic oral administration of the toxic nucleosides exacerbated the model leading to the manifestation of neurological phenotype and thus providing a better tool to test therapeutic intervention. In this study, we show that AAV-mediated gene therapy prevents the enlargement of brain ventricles and the neuromotor dysfunction observed in the mice. Hence, we prove that liver-targeted gene therapy using an AAV vector prevents the manifestation of a neurological phenotype beyond correcting the biochemical nucleoside imbalance. This is the first time liver-targeted AAV-mediated gene therapy for MNGIE shows efficacy on clinical parameters in the animal model of the disease, which constitutes an important step towards the translation of this therapy to patients.

### Implications of all the available evidence

At present, hematopoietic stem cell transplantation and liver transplantation are the only available therapies for MNGIE patients. However, both treatments are constrained by the availability of a suitable donor and involve complex medical interventions associated to life-threatening risks. Gene therapy may constitute a safer alternative, and this study provides evidence that liver targeted AAV-mediated gene therapy is effective on the neurological phenotype in the enhanced animal model of the disease. This will support conducting clinical studies that will bring this potential treatment closer to patients.

transplant-related complications, which are aggravated in MNGIE patients by the poor clinical condition when most are treated [13]. More recently, orthotopic liver transplantation was proposed as an alternative option [14], and the reported cases indicate that successful engraftment results in a sustained nucleoside reduction [15–18]. However, liver transplantation is also an aggressive intervention, and it is constrained by a limited supply of donors.

Over the last few years, several preclinical studies have proven the effectiveness of lentiviral hematopoietic stem cell gene therapy or liver-targeted adeno-associated virus (AAV) vector gene therapy to correct MNGIE biochemical disarrangements in a *Tymp/Upp1* double knockout (dKO) mouse model of the disease [5,19–24]. However, as the dKO mouse model has a limited and elusive functional phenotype except for its clear metabolic imbalances, these preclinical studies have relied almost exclusively on demonstrating correction of the biochemical imbalances caused by the lack of TP activity. It has been shown that chronic oral administration of dThd and dUrd to dKO mice significantly enhances the phenotype beyond biochemical derangements and provides a better model to test therapy approaches [25]. Taking advantage of this improved model, we show here that the liver-targeted AAV gene therapy not only corrects the biochemical imbalances of the nucleoside-stressed model, but also prevents other functional changes such as those related to its neurological phenotype.

## 2. Methods

### 2.1. Vector construction, production, and titration

The human coding sequence of *TYMP* (hcTYMP) was cloned in three different vectors (AAV-TBG, AAV-AAT, and AAV-HLP) and packaged in AAV8 serotype as previously described [19]. AAV-TBG contained hcTYMP under regulation of the thyroxine binding globulin (TBG) promoter in a single-stranded configuration. AAV-AAT contained hcTYMP under regulation of the  $\alpha$ -1-antitrypsin promoter and the apolipoprotein E hepatic control region (ApoE-AAT cassette) in a single-stranded configuration. AAV-HLP contained hcTYMP under regulation of the hybrid liver-specific promoter, which is composed of an abbreviated form of the ApoE-AAT cassette [26] in a self-complementary configuration. For construction of AAV-HLP, the pAV-HLP-Luc plasmid was provided by Dr. Nathwani's group (University College London Cancer Institute, London, United Kingdom) and the luciferase gene was replaced by the hcTYMP sequence. All vectors were produced and titrated as indicated elsewhere [19].

### 2.2. Animal procedures

All animal procedures were conducted in accordance with the rules established by the *Generalitat de Catalunya* for the Care and Use of Laboratory Animals and in compliance with the ARRIVE guidelines. The protocols were approved by the Ethics Committee for Animal Experimentation of the Vall d'Hebron Research Institute (Permit Number: 14–06).

A double knockout mouse for the genes *Tymp* and *Upp1* previously described was used for this study [5]. AAV transduction efficiency in mice is higher in males than females [27]. Thus, to avoid sex-related variation in the results, only male animals were used in this study.

For chronic oral nucleoside exposure (“exposed” mice), the animals' drinking water was supplemented with 16.6 g/L of dThd and dUrd (68.6 mM dThd and 72.3 mM dUrd) from weaning up to the end of the study (22-month-old mice) [25]. Mice that were not exposed to nucleoside administration are designated as “naïve” in this study.

To study pharmacokinetics (PK) following acute nucleoside administration (peak plasma concentration, area under the curve

weakness, and diffuse leukoencephalopathy on brain magnetic resonance imaging (MRI). Disease onset is usually between the first and fifth decades, in most cases before the age of 20 years, and the condition progressively degenerates, causing premature death of affected patients usually during the third to fourth decade of life [9].

Several therapeutic strategies have been proposed for MNGIE, all of them addressed to reducing the toxic nucleoside accumulation [10]. Allogeneic hematopoietic stem cell transplantation was the first treatment providing a permanent nucleoside reduction and clinical improvement or stabilization in patients [11,12]. However, it is an aggressive therapy associated with a high mortality risk due to

[AUC], time to reach plasma concentration in naïve wild type [WT] animals), a single dose was administered by oral gavage (10  $\mu$ L/g body weight of 16.6 g/L of dThd and dUrd aqueous solution, ie, 166 mg dThd + 166 mg dUrd/kg body weight). Blood samples were collected immediately before nucleoside administration, and at 30 min, 1 h, 1.5 h, 2 h, 3 h, 5 h, and 8 h after administration. In the PK study, mice were deprived of access to drinking water during the first 3 h after gavage.

To detect the influence of possible metabolic adaptation on PK in chronically dThd/dUrd-treated mice (exposed group), acute dThd/dUrd administration was studied under two different conditions: mice without chronic oral dThd/dUrd treatment (naïve group), and mice already receiving chronic dThd/dUrd treatment (exposed group). In this latter case, dThd/dUrd was withdrawn from drinking water 24 h before acute administration for the PK study.

Therapeutic vectors were administered to 8- to 11-week-old dKO mice in a single intravenous injection (tail vein) of AAV-TBG at doses (in vector genomes per kg, vg/kg) of  $5 \times 10^{11}$ ,  $10^{12}$ ,  $2 \times 10^{12}$  and  $10^{13}$ , and AAV-AAT or AAV-HLP, both at doses of  $2 \times 10^{12}$  and  $10^{13}$ .

Blood samples from live animals were collected from the saphenous vein using EDTA capillaries (Microvette 200K3E, Sarstedt). At the end of the study (age 22 months), mice were euthanized by cervical dislocation. Heart blood was immediately collected in EDTA-treated tubes, and tissues (liver, brain, small intestine and gastrocnemius skeletal muscle) were excised and immediately frozen in liquid nitrogen and stored at  $-80^{\circ}\text{C}$ . Before analysis, mouse tissues were ground to a fine powder with a ceramic mortar and pestle without defrosting in liquid nitrogen.

### 2.3. TP activity and nucleoside determination

Plasma dThd and dUrd concentrations were determined by HPLC-UV, as previously described [22]. For TP activity, 100–200  $\mu$ g of pulverized tissue was homogenized with a plastic pestle in 800  $\mu$ L of lysis buffer. Homogenates were centrifuged at 20,000  $\times$  g for 30 min at  $4^{\circ}\text{C}$ , the supernatant protein concentration was measured [28], and TP activity was determined as described elsewhere [29].

For dThd and dUrd quantification in tissue, 100–200  $\mu$ g of pulverized samples was homogenized with a plastic pestle in lysis buffer with addition of 1  $\mu$ M internal standard (isotope-labeled dThd:  $^{13}\text{C}_{10}$ - $^{15}\text{N}_2$ -dThd) and TP activity inhibitors to prevent in vitro degradation of nucleosides in homogenates: 100  $\mu$ M of 5-chloro-6-[1-(2-iminopyrrolidinyl) methyl] uracil hydrochloride (strong TP-specific inhibitor that does not inhibit uridine phosphorylase (UP), used in liver homogenates containing high TP activity derived from AAV transduction) or 100  $\mu$ M 6-amino-5-bromouracil (TP and UP inhibitor) and 100  $\mu$ M tetrahydrouridine (cytidine deaminase inhibitor), used in small intestine homogenates containing high TP and UP activity) [30]. Homogenates were centrifuged at 20,000  $\times$  g for 30 min at  $4^{\circ}\text{C}$ , and protein concentration of the supernatant was measured [28]. The supernatant was deproteinized by ultrafiltration (10 kDa Amicon Ultra filters; Merck Millipore) at 14,000  $\times$  g for 30 min at  $4^{\circ}\text{C}$ . The ultrafiltrate was later used to measure nucleosides by LC-MS/MS (liquid chromatography coupled to tandem mass spectrometry). Components of the sample were resolved and detected as previously described [23]. Serial dilutions of dThd and dUrd standards (0.5–20  $\mu$ M) in lysis buffer and 1  $\mu$ M of internal standard were processed in parallel to generate calibration curves. dThd and dUrd concentrations in the samples were obtained from interpolation of the peak areas relative to the internal standard in the calibration curve.

### 2.4. Vector copy number determination

DNA was isolated with phenol-chloroform from approximately 25 mg of frozen liver and dissolved in 10 mM Tris-HCl, pH 8.0. Vector genome copies per cell were quantified by qPCR on the 7900HT Fast

Real-Time PCR System (Applied Biosystems). hcTYMP DNA copy number was quantified using the predesigned TaqMan MGB expression assay Hs00157317\_m1 and referred to the murine single-copy nuclear gene *Ang1* using the predesigned TaqMan MGB gene expression assay Mm00833184\_s1 as previously described [19]. Quantifications were based on a standard curve prepared with different dilutions of plasmids containing hcTYMP DNA or a specific region of the *Ang1* gene.

### 2.5. Motor performance

Motor coordination, balance and exercise tolerance were assessed in 25-week-old mice by testing their time to fall in a rotarod apparatus (Ugo Basile Mouse Rota-Rod). The protocol included three training sessions of 2 min each at a constant 4-rpm speed prior to the test. The test session was then started at a speed of 4 rpm for 15 s, followed by a constant acceleration rate of 1 rpm/s for 45 s. Three test sessions were carried out with each mouse and the three time-to-fall values were recorded and averaged [25].

### 2.6. Magnetic resonance imaging

Eighteen months-old mice were anesthetized with 4% (v/v) and maintained with 1.5% (v/v) isoflurane in  $\text{O}_2$  at 1 L/min. Mice were placed in prone position on a water-jacketed bed to maintain body temperature ( $37 \pm 1^{\circ}\text{C}$ ) and immobilized with bite-bar and ear-bars. Stable respiration rate (50–80 bpm) and rectal temperature were monitored (SA Instruments, Stony Brook, NT).

$^1\text{H}$ -MRI studies were performed at the joint nuclear magnetic resonance facility of the Universitat Autònoma de Barcelona and Centro de Investigación Biomédica en Red—Bioingeniería, Biomateriales y Nanomedicina (CIBER-BBN) (Cerdanyola del Vallès, Catalonia), Unit 25 of NANBIOSIS. Experiments were conducted on a 7T Bruker BioSpec 70/30USR scanner (Bruker BioSpin GmbH, Ettlingen, Germany) equipped with a 72-mm inner diameter linear volume coil as a transmitter and a dedicated mouse brain surface coil as a receiver. MRI data were acquired and processed on a Linux computer using Paravision 5.1 software (Bruker BioSpin GmbH, Karlsruhe, Germany).

Low-resolution  $\text{T}_2$ -weighted fast spin-echo images were initially obtained in axial, sagittal, and coronal planes for use as reference scout images. The following imaging parameters were applied: TE (effective echo time) 36 ms; TR (repetition time) 2 s; ETL (echo train length) 8; FOV (field of view)  $1.92 \times 1.92 \text{ cm}^2$ ; MTX (matrix size)  $128 \times 128$ ; ST (slice thickness) 1 mm; gap (gap between slices) 0.1 mm; NS (number of slices) 14 axial, 9 sagittal, 5 coronal; NA (number of averages) 1; and Expt (experiment time) 24 s per orientation.

$\text{T}_2$  maps were acquired using a multi-spin multi-echo sequence.  $\text{T}_2$ -weighted images at 24 different TE values between 10 and 240 ms were acquired, with TR 3 s, FOV  $1.92 \times 1.92 \text{ cm}^2$ , MTX  $128 \times 128$ , NS 8, ST 1 mm, and gap 0.1 mm, covering the whole brain excluding the olfactory bulb and cerebellum (Supp. Figure 6a), with Expt 4 min 48 s.

Voxel-wise  $\text{T}_2$  relaxation maps were calculated using Paravision 5.1 software. Regions of interest corresponding to the total brain and excluding ventricular areas were manually outlined for each slice and the mean  $\text{T}_2$  region values were calculated for each mouse.

For ventricular volume measurement, brain volume was manually outlined in each slice. Within the selected brain region, ventricular pixels were automatically pre-defined on  $\text{T}_2$  maps as pixels having  $\text{T}_2$  values above 60 ms. The analysis was reviewed and non-ventricular regions were manually removed. The sum of ventricular pixels in all slices was then multiplied by the voxel volume ( $0.15 \times 0.15 \times 1 \text{ mm}^3$ ) to provide the total ventricular volume for each mouse.

## 2.7. Mitochondrial isolation and dNTP determination

Liver and brain mitochondria were isolated and dNTPs were extracted as previously described [4,19]. For dNTP quantification, dry extracts were thawed and re-dissolved in 40  $\mu$ L of 40 mM Tris–HCl, pH 7.4. Mitochondrial dNTP content was determined using the previously described polymerase-based method [31] with some modifications [19].

## 2.8. Mitochondrial DNA copy number analysis

Total DNA was isolated from approximately 25 mg of pulverized frozen tissue with the QIAamp DNA Mini Kit (Qiagen) and dissolved in 10 mM Tris–HCl (pH 8). MtDNA copy number was quantified by qPCR on the 7900HT Fast Real Time PCR System (Applied Biosystems) using a probe targeted to the mitochondrial gene *mt-Rnr2* (encoding the 16S rRNA) and referred to the nuclear gene *Ang1*, following the protocol detailed elsewhere [32].

## 2.9. Histochemical staining of small intestine

Longitudinal sections of jejunum were analysed using the adapted “Swiss roll” technique [33]. Jejunum sections were fixed in 4% neutral buffered formalin and embedded in paraffin for histological examination. Three- $\mu$ m-thick slices were stained with Masson’s trichrome. Images were taken using a FSX100 fluorescence microscope and the software FSX-BSW (Olympus, Tokyo, Japan).

## 2.10. Statistical analysis

Statistical analyses were performed using the GraphPad Prism 6 program (GraphPad Software, Inc.). For multiple comparisons (multiple comparisons with one reference group, and multiple comparisons of all groups compared with each other) the Kruskal-Wallis test followed by the Dunn’s multiple comparisons test was used. When the only interest was to compare two groups defined by only one variable (e.g., exposed group vs. non-exposed group), we used the Mann-Whitney *U* test. In any case, tests used are always indicated in the figure legends. For statistical purposes, undetectable values were considered as zero. Nucleoside PK parameters, including peak plasma concentration, AUC, and time to reach plasma WT concentration, were calculated from the graphical curves obtained by plotting nucleoside plasma concentrations vs time, defined by connecting adjacent measurements with straight lines, and taking as baseline the mean plasma nucleoside concentration at time 0 h in naïve WT mice.

## 2.11. Role of funding source

The disclosed funders had no role in study design, data collection and analysis, interpretation, decision to publish, or preparation of the manuscript.

## 3. Results

### 3.1. Pharmacokinetics of dThd and dUrd in the murine model

In agreement with previous reports [19–24], in the absence of oral nucleoside administration (naïve mice), circulating dThd and dUrd concentrations were around 3-fold higher in dKO mice than in WT mice (Fig. 1a and Supplementary Fig. 1). A marked increase in plasma dThd and dUrd concentrations above normal WT levels was observed in the exposed groups. When the time of blood sample collection was not considered, plasma dThd and dUrd concentrations showed wide dispersion in the exposed groups (data not shown). This variability was greatly reduced after changing the protocol and collecting all

blood samples between 8 and 9 am (8- to 30-fold increase in exposed WT mice, and 13- to 26-fold increase in exposed dKO mice) (Fig. 1a and Supplementary Fig. 1). As mice were exposed to dThd and dUrd in drinking water *ad libitum*, it was not possible to determine the time of the last intake before blood collection. This may account for the wide, randomly distributed variation in plasma concentrations; that is, time differences between the last water intake and sample collection.

Thus, we decided to explore a more controlled set of parameters, by studying nucleoside PK in 35 to 40 week-old mice after a single dThd/dUrd administration by oral gavage in naïve WT and dKO mice. We also studied exposed WT and dKO mice to detect whether a possible metabolic adaptation in response to chronic dThd and dUrd exposure influenced PK. After the single oral dose, plasma concentrations rose above naïve dKO levels, reaching a peak value between 1 and 1.5 h after oral gavage (Fig. 1b and Supplementary Fig. 2a). Thereafter, deoxyribonucleoside (dN) levels rapidly declined, even in dKO mice, which lack the required catabolic enzymes, owing to urinary excretion (data not shown). Eight hours after oral administration, dThd and dUrd plasma levels remained above normal plasma levels in all groups. Peak concentrations (Fig. 1c and Supplementary Fig. 2b) and AUCs (Fig. 1d and Supplementary Fig. 2c) showed a clear tendency to be higher in dKO mice than WT mice, in both the naïve and exposed groups, respectively. We also found that AUC values were higher in exposed dKO than in naïve dKO mice (Fig. 1d and Supplementary Fig. 2c).

### 3.2. AAV-TYMP treatment limits nucleoside stress in chronically dThd/dUrd-exposed dKO mice

Exposed dKO mice were treated with three different liver-targeted AAV vectors carrying hcTYMP (AAV-TBG, AAV-AAT, or AAV-HLP) at different doses. Plasma dThd and dUrd monitoring over 35 weeks showed the following: although AAV treatment failed to reduce circulating levels of these nucleosides at most time points, the frequency of randomly distributed samples in which nucleoside concentrations decreased to levels within the range of naïve dKO mice (Supplementary Fig. 3) was higher than that of untreated exposed dKO mice (Fig. 1a). As the last nucleoside intake (in drinking water) before blood sample collection might have been interfering with detection of the effect of AAV treatment on dN concentration, we analyzed the effect of AAV treatment on PK parameters in gavage-exposed dKO mice (Fig. 1b–e). Before gavage dosing, plasma dThd and dUrd concentrations in all AAV-treated mice but one were in the WT range or below (dThd, 1.9–3.5  $\mu$ M; dUrd, 2.5–4.2  $\mu$ M). It should be noted that the group of exposed mice had been deprived of oral dThd and dUrd in drinking water 24 h before PK assessment. AAV treatment reduced peak dThd concentrations to well below the peak concentrations observed in exposed dKO mice, regardless of the vector construct or dose used, although statistical significance was not reached for the two AAV-TBG lowest doses (Fig. 1c). AAV treatment led to even more pronounced reductions in the AUC (Fig. 1d). In contrast to what occurred in AAV-untreated mice, which did not reach WT nucleoside levels after gavage nucleoside administration over 8 h of monitoring (Fig. 1b), all AAV-treated exposed dKO mice reached WT levels in less than 8 h (Fig. 1e). A dose-dependent effect in the time reduction to reach WT dThd concentration was observed with all vectors; a similar, but less marked dose-dependent effect was observed on peak dThd concentration and dThd AUC. Comparison between the different vectors showed that AAV-AAT had the most pronounced effect on dThd PKs.

The greatest effect was achieved with AAV-AAT at  $10^{13}$  vg/kg, which reduced plasma dThd concentration to  $<3.5$   $\mu$ M in a mean of 2.2 h (range 1.8–2.6 h) after oral gavage. Mice treated with  $10^{13}$  vg/kg of AAV-AAT also showed the lowest mean dThd peak concentration (13.8  $\mu$ M, range 5.5–16.9) and the lowest mean

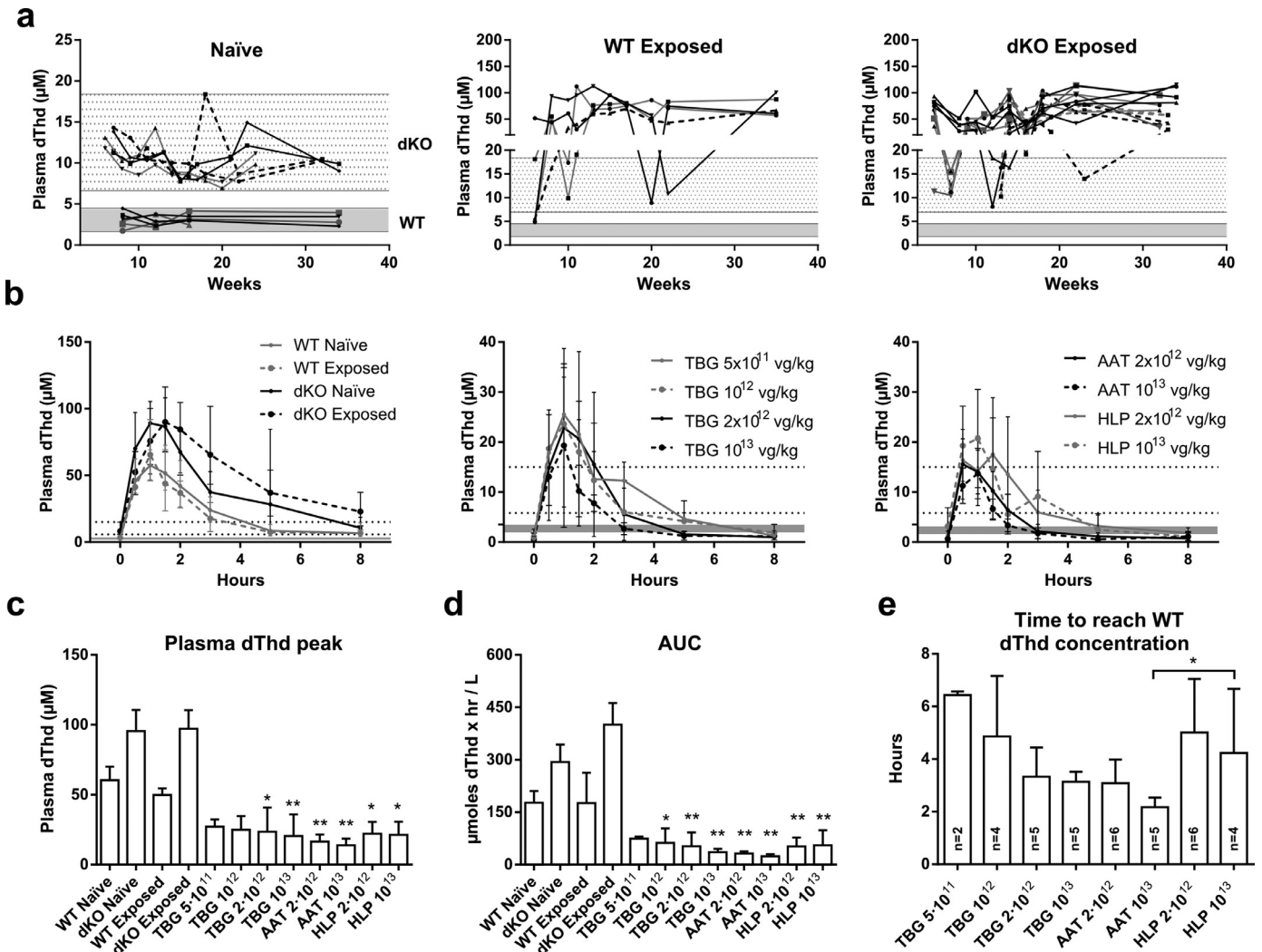


**Fig. 1.** Effect of AAV treatment on dThd pharmacokinetics. **a**) Plasma dThd concentration in WT and dKO mice exposed to dThd and dUrd supplementation in drinking water starting from weaning (exposed group), or without exposure (naïve group), until 5 to 34 weeks of age. The monitored range encompasses 5 to 34 weeks of age. Each symbol and line represents a single mouse. Gray dotted and shadowed areas indicate the concentration range in naïve dKO and WT groups, respectively. **b**) Plasma dThd concentrations before (0 h) and after a single administration of dThd and dUrd by oral gavage (166 mg/kg each) in naïve and exposed WT mice, naïve and exposed dKO mice, and exposed dKO mice previously treated with different doses of AAV-TBG, AAV-AAT and AAV-HLP vectors. Mice were 35 to 45 weeks old at the time of the experiment. Each point represents mean $\pm$ range. White and gray areas between dotted lines indicate the concentration range in naïve dKO and WT groups at time zero, respectively. **c**, **d** and **e**) PK results (mean $\pm$ SD) obtained from experiments depicted at **b**. Sample sizes in panels **b** to **e** are: naïve WT,  $n = 8$ ; naïve dKO,  $n = 6$ ; exposed WT,  $n = 5$ ; exposed dKO,  $n = 7$ ; TBG-treated mice with  $5 \times 10^{11}$  vg/kg  $n = 2$ ,  $10^{12}$  vg/kg  $n = 4$ ,  $2 \times 10^{12}$  vg/kg  $n = 5$ , and  $10^{13}$  vg/kg  $n = 5$ ; AAT-treated mice with  $2 \times 10^{12}$  vg/kg  $n = 6$  and  $10^{13}$  vg/kg  $n = 5$ ; HLP-treated mice with  $2 \times 10^{12}$  vg/kg  $n = 6$  and  $10^{13}$  vg/kg  $n = 4$ . Asterisks indicate statistically significant differences ( $*p < 0.05$ ,  $**p < 0.01$ ; panels **c** and **d**, Kruskal-Wallis test followed by the Dunn's multiple comparisons test, all groups compared with dKO exposed; panel **e**, Kruskal-Wallis test followed by the Dunn's multiple comparisons test, all groups compared with each other). AUC, area under the curve.

dThd AUC (23.8  $\mu\text{moles dThd} \times \text{hour/L}$ , range 15.8–29.3). Similar effects of AAV treatment on PK were observed for dUrd (Supplementary Fig. 2).

Nucleoside-exposed mice were treated with dThd/dUrd in drinking water from weaning until the end of the study (at 22 months old). At this point, mice were killed and dThd and dUrd levels were analyzed in plasma and liver (AAV target organ), as well as brain and small intestine (two affected organs in MNGIE patients). Chronic oral nucleoside exposure resulted in increased dThd median levels in all tissues in WT mice (plasma 5-fold, liver 2-fold, brain 4-fold, and small intestine 90-fold, as compared with median levels in naïve WT group), and showed a higher increase in dKO mice (plasma 20-fold, liver 10-fold, brain 7.5-fold, and small intestine 275-fold, as compared with median levels in naïve WT group) (Fig. 2). In addition, AAV-treatment reduced dThd and dUrd levels in nucleoside-exposed mice at the end of the study in liver (reductions compared to exposed dKO AAV-untreated, with levels comparable to those of WT naïve mice) and in brain (reductions compared to untreated exposed dKO

AAV, with levels comparable to those of exposed WT mice in all groups and doses except the lowest AAV-TBG dose). In plasma, reductions were especially prominent in mice treated with the AAV-AAT vector (and reached statistical significance for the dose  $2 \times 10^{12}$  vg/kg), whereas there was no effect in small intestine with any treatment. The greatest reductions were obtained for the AAV-AAT vector in plasma, liver, and brain. Similar results were observed for the dUrd concentrations (Supplementary Fig. 4).

### 3.3. AAV-TYMP treatment induces increased TP activity in liver

Chronic nucleoside exposure induced increased TP activity in liver tissue in WT mice (mean value 39 nmoles Thy/h/mg prot in naïve WT, and 112 in exposed WT), and in dKO mice (mean value 1.2 in naïve dKO, and 9.9 in exposed dKO) (Fig. 3a), but not in small intestine, brain, or skeletal muscle (Supplementary Fig. 5). Treatment with AAV vectors provided TP activity to liver of exposed mice in a dose-dependent manner (Fig. 3b). AAV-AAT was the most effective vector

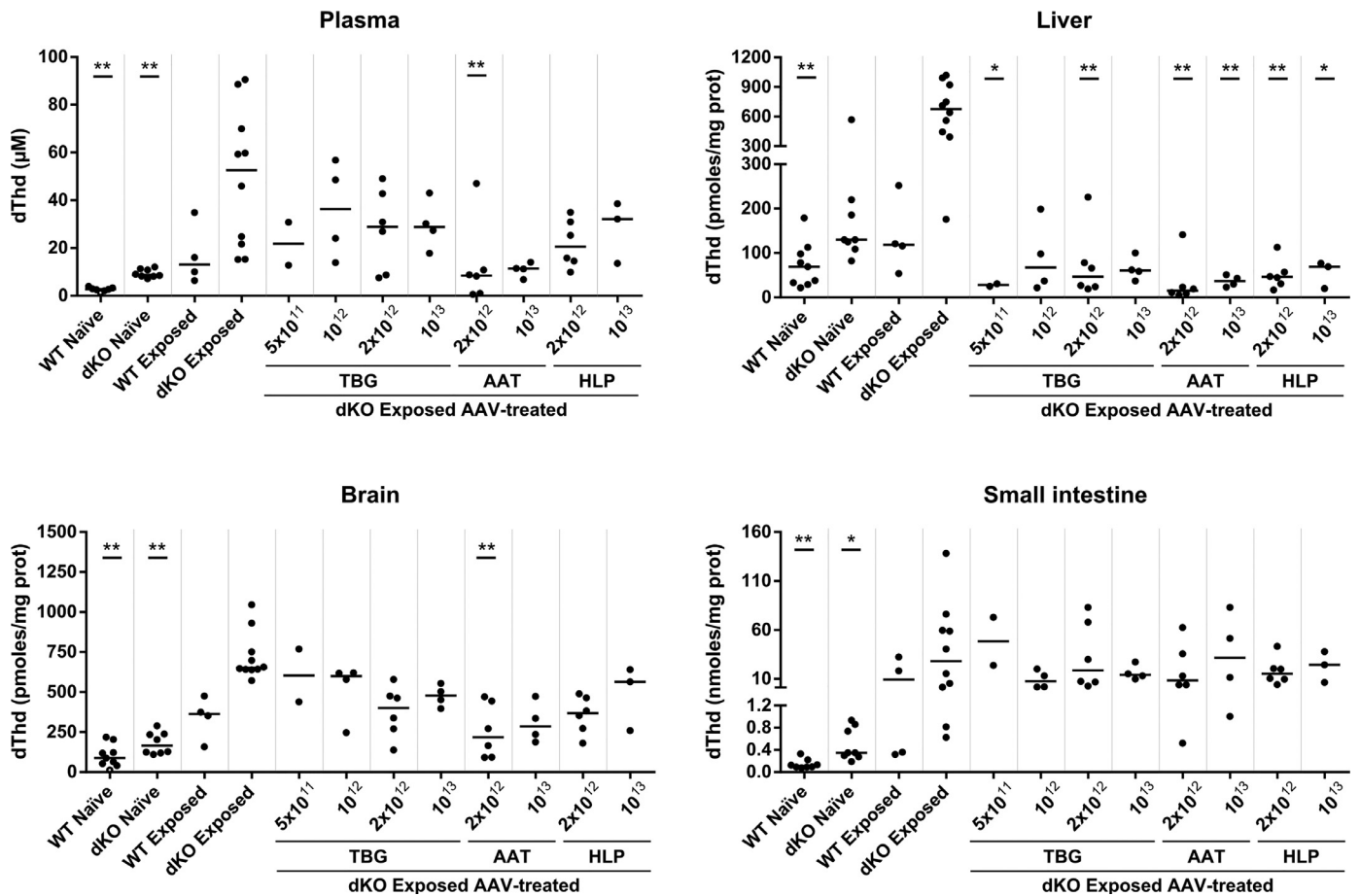


**Fig. 2.** Effect of AAV treatment on dThd levels in 22-month-old mice. Plasma, liver, brain, and small intestine dThd concentration in WT ( $n = 7-9$ ) and dKO ( $n = 8$ ) naïve mice, WT ( $n = 4$ ) and dKO ( $n = 10$ ) exposed mice, and dKO exposed mice treated with different AAV doses (TBG-treated mice with  $5 \times 10^{11}$  vg/kg  $n = 2$ ,  $10^{12}$  vg/kg  $n = 4$ ,  $2 \times 10^{12}$  vg/kg  $n = 6$  and  $10^{13}$  vg/kg  $n = 4$ ; AAT-treated mice with  $2 \times 10^{12}$  vg/kg  $n = 6$  and  $10^{13}$  vg/kg  $n = 4$ ; HLP-treated mice with  $2 \times 10^{12}$  vg/kg  $n = 6$  and  $10^{13}$  vg/kg  $n = 3$ ). Horizontal lines indicate the median concentration for each group. Asterisks indicate statistically significant differences (\* $p < 0.05$ , \*\* $p < 0.01$ ; Kruskal-Wallis test followed by the Dunn's multiple comparisons test, all groups compared with dKO exposed).

in providing TP activity to liver, in agreement with its nucleoside reduction. At the highest dose ( $10^{13}$  vg/kg), liver TP activity mean values in exposed mice increased 40- to 75-fold compared to WT values:  $2091 \pm 140$  nmoles Thy/h/mg prot for AAV-TBG (mean  $\pm$  SD);  $3031 \pm 509$  for AAV-AAT and  $1535 \pm 456$  for AAV-HLP (Fig. 3b).

Vector copy number (VCN) increased in liver in a dose-dependent manner (Fig. 3c). In an attempt to compare the efficacy of the promoters carried by the three vectors, we normalized TP activity per VCN, and the results revealed that TP/VCN ratios were not constant for each vector, but declined as VCN increased (Fig. 3d). This apparent "saturation of efficacy" makes it difficult to compare the efficacies of different promoters, but the fact that the highest TP/VCN ratios were always observed with the AAV-AAT vector for all different VCN values (Fig. 3d), suggests that AAT was the most effective promoter among those tested. The TP vs VCN distribution was adjusted to the nonlinear function:  $Y = \text{intercept} + \text{slope} \times \log(X)$ , where Y is TP activity and X is VCN. Semilogarithmic transformation of the function showed that the highest slope among the three vectors corresponded to AAV-AAT ( $p < 0.05$ , extra sum of squares F-test).

Although all the promoters used here are liver-specific, AAV treatment provided TP activity to small intestine in exposed dKO mice, as well as skeletal muscle treated with the highest vector doses, and brain in a few individual mice. AAV-induced TP activities did not reach levels above WT values in non-hepatic tissues except in a single skeletal muscle sample (Supplementary Fig. 5).

#### 3.4. Histological analysis of small intestine and mtDNA copy number

Histological analysis of the small intestine (Masson's trichrome staining) did not reveal any detectable abnormalities induced by nucleoside exposure in this tissue. Also, we could not find that nucleoside exposure induced mtDNA depletion in brain and small intestine. (Supplementary figure 6).

#### 3.5. Effect of the AAV-TYMP treatment on neurological phenotype

Motor coordination, balance and exercise tolerance were determined using the rotarod performance test in 25 week-old mice (Fig. 4). The performance in this test can be influenced by impaired function of the skeletal muscles and/or the central nervous system. Multiple comparison analysis of all groups represented in Fig. 4 (Kruskal-Wallis test, followed by the Dunn's multiple comparisons test) did not detect statistical differences for any group, probably due to the high number of groups. However, when we only analysed the effect of nucleoside exposition, we observed that exposed dKO mice had a reduced time to fall, as compared with WT naïve mice ( $p = 0.006$ , Mann-Whitney U test) (Fig. 4). In AAV-treated mice, rotarod performance varied widely, but in most AAV-treated mice (69%; 27 out of 39) was within or above the naïve WT normal range (19–44 s), whereas only 33% (3 out of 9) of exposed dKO mice showed a lengthier time to fall.

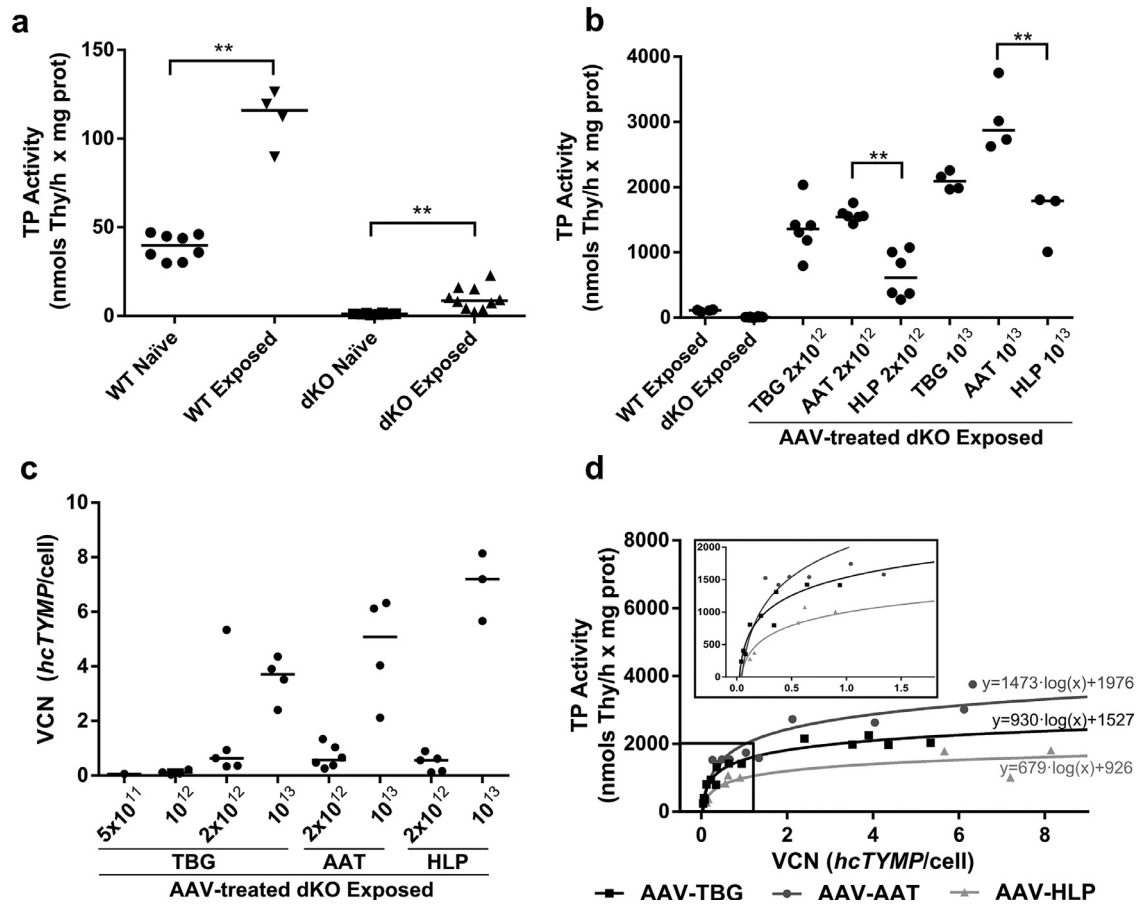


**Fig. 3.** TP activity in liver after AAV treatment. Liver TP activity in (a) WT ( $n = 8$ ) and dKO ( $n = 8$ ) naïve mice and in untreated WT ( $n = 4$ ) and dKO ( $n = 10$ ) exposed mice. (b) Liver TP activity in untreated WT and dKO exposed mice and in dKO exposed mice treated with different AAVs doses (TBG-treated mice with  $5 \times 10^{11}$  vg/kg  $n = 2$ ,  $10^{12}$  vg/kg  $n = 4$ ,  $2 \times 10^{12}$  vg/kg  $n = 6$  and  $10^{13}$  vg/kg  $n = 4$ ; AAT-treated mice with  $2 \times 10^{12}$  vg/kg  $n = 6$  and  $10^{13}$  vg/kg  $n = 4$ ; HLP-treated mice with  $2 \times 10^{12}$  vg/kg  $n = 6$  and  $10^{13}$  vg/kg  $n = 3$ ). (c) Liver vector copy number (VCN) in AAV-treated dKO exposed mice. TBG-treated mice with  $5 \times 10^{11}$  vg/kg  $n = 1$ ,  $10^{12}$  vg/kg  $n = 4$ ,  $2 \times 10^{12}$  vg/kg  $n = 5$  and  $10^{13}$  vg/kg  $n = 4$ ; AAT-treated mice with  $2 \times 10^{12}$  vg/kg  $n = 6$  and  $10^{13}$  vg/kg  $n = 4$ ; HLP-treated mice with:  $2 \times 10^{12}$  vg/kg  $n = 5$  and  $10^{13}$  vg/kg  $n = 3$ . Horizontal lines indicate the median for each group. (d) Non-linear regression of liver TP activity (data from panel b) vs. liver VCN (data from panel c) in AAV-treated mice ( $Y = \text{intercept} + \text{slope} \times \log(X)$ ). Note that the low VCN region is magnified to facilitate observation of the differences between the three vectors. Asterisks indicate statistically significant differences ( $*p < 0.05$ ,  $**p < 0.01$ ; for panel a, Mann-Whitney U test; for panel b, Kruskal-Wallis test followed by the Dunn's multiple comparisons test, all groups compared with each other, two different analyses for each dose).

All MNGIE patients have diffuse leukoencephalopathy on brain MRI [9], and chronic oral exposure to dThd and dUrd enhances leukoencephalopathy in the dKO murine model [25]. We performed brain MRI studies in 84-week-old naïve and exposed WT and dKO mice. Larger T2-weighted hyperintense areas (indicative of cerebrospinal fluid) were found in exposed dKO mice than in naïve dKO, naïve WT, or exposed WT mice (Fig. 5a and Supplementary Fig. 7). In contrast to what was reported in the former study of nucleoside exposed dKO mice, we did not find leukoencephalopathy in our experimental setting, probably because of different magnetic resonance protocols [25]. Hyperintensity was mainly located in the third and lateral ventricles, suggesting ventricular enlargement. The volume of the third and lateral ventricles was quantified using T2 maps, and it was significantly greater in exposed dKO mice than in naïve WT mice whereas it was unchanged in both naïve dKO and exposed WT mice (Fig. 5b). AAV-AAT and AAV-HLP treatment prevented ventricular enlargement in exposed dKO mice: most animals treated with these vectors had normal ventricular volumes, with the exception of one mouse treated with  $10^{13}$  vg/kg AAV-AAT that developed hydrocephalus. In contrast, AAV-TBG failed to prevent ventricular enlargement in most cases (Fig. 5b).

Ventricular volumes at 84 weeks of age significantly correlated with brain dThd levels at the end of the study (94 weeks) in all groups (Spearman  $r = 0.324$ ,  $p = 0.014$ ,  $n = 57$ , excluding 2 ventricular volume

extreme values;  $r = 0.358$ ,  $p = 0.005$ ,  $n = 59$ , including all values) and with rotarod test performance (Spearman  $r = -0.348$ ,  $p = 0.0068$ ,  $n = 59$ , excluding two ventricular volume extreme values). Ventricular volumes did not significantly correlate with plasma or liver dThd levels.

### 3.6. AAV-TYMP treatment normalized the mitochondrial dNTP balance

In MNGIE, nucleoside overload leads to an unbalanced dNTP mitochondrial pool, resulting in mtDNA instability [4]. We quantified dNTP levels in mitochondrial extracts from liver and brain in 22-month-old mice (Fig 6). dTTP content was significantly increased in brain mitochondria of exposed dKO mice. The same trend was observed in liver mitochondria, but statistical significance was not reached, probably owing to the wide dispersion of the values (liver dTTP range: 5.3–54.7 pmoles/mg protein). The dTTP expansion in liver was largely prevented in exposed dKO mice treated with AAVs, as most values of AAV treated mice returned to dTTP values with the naïve WT range, although only the group treated with AAV-TBG at  $10^{13}$  vg/kg reached statistical significance (Fig. 6a). AAV treatment also limited dTTP expansion in brain, but the effect was only partial as dNTP in AAV-treated animals did not reach WT levels (and reached statistical significance only in the group treated with AAV-AAT at  $2 \times 10^{12}$  vg/kg) (Fig. 6b). The observations regarding mitochondrial

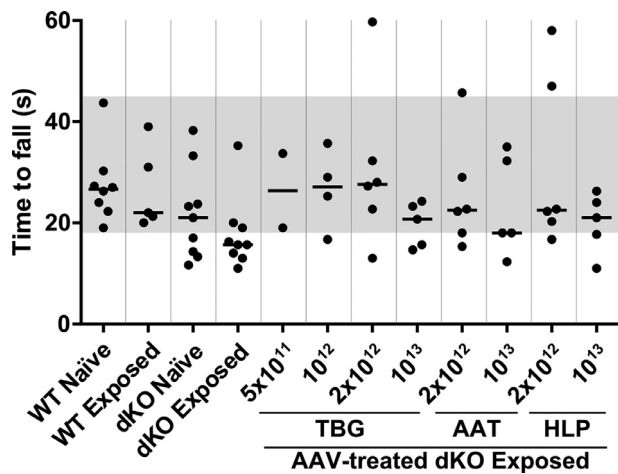


**Fig. 4.** Motor function. Motor function assessed by rotarod test in 25-week-old WT and dKO naïve and exposed mice, and dKO exposed mice treated with different AAVs doses. Horizontal lines show median time to fall in each group. Gray areas indicate the range of values in the naïve WT group. No statistical differences found, Kruskal-Wallis test followed by the Dunn's multiple comparisons test, all groups compared with dKO exposed).

dCTP levels in liver conversely mirrored those of dTTP; that is, exposed dKO showed dCTP depletion as compared with WT levels, which was largely prevented by AAV treatment, reaching statistical significance for all AAV-AAT treated groups, and for the group treated with AAV- HLP at  $2 \times 10^{12}$  vg/kg (Fig. 6c). No statistical differences were detected in mitochondrial dCTP levels in brain (Fig. 6d). As to the purine deoxynucleotides, mitochondrial dGTP levels were expanded in liver (an increase that was not prevented by AAV treatment), while dATP showed a tendency to be depleted in the same organ (statistically non-significant), but the effect was prevented in most AAV treated groups. In contrast, mitochondrial dATP and dGTP levels were barely affected or not affected at all in brain (Supplementary Fig. 8).

#### 4. Discussion

Over the last few years, gene therapy has been proposed to reduce the relevant risks associated with the currently available options to treat MNGIE (allogeneic stem cell transplantation and orthotopic liver transplantation) [11–13,15–18,34]. Since the first proof-of-concept preclinical studies demonstrating the feasibility of using lentiviral [22] and AAV vectors [23], several studies have shown that these strategies provide maintained effectiveness at long term in the preclinical model [19–21,24]. The main endpoint used to draw conclusions was the ability of the vectors to achieve genetic correction in target cells of the murine dKO model, thereby providing TP activity and normalization of systemic dThd and dUrd levels.

However, the dKO mouse is a limited model due to the absence of a clinically relevant phenotype, which consists of a lack of TP activity (except for some residual activity in tissues expressing *Upp2*), moderate dThd and dUrd systemic accumulation, and a modest mitochondrial dNTP imbalance. Any additional traits beyond the biochemical consequences of the absence of TP have only been glimpsed in very old animals and, even so, as elusive and barely detectable signs [5]. The model can be enhanced by providing the animals with dThd and dUrd in drinking water, which exacerbates the phenotype and highlights the importance of dThd and dUrd overload in the pathophysiology of MNGIE [25]. This enhanced model does not recapitulate the main clinical features of the disease (which manifest mainly as severe gastrointestinal dysmotility, myopathy, peripheral neuropathy and brain diffuse leukoencephalopathy). Specifically, the lack of gastrointestinal phenotype is an important limitation of this animal model,

because gastrointestinal dysmotility is the most debilitating symptom in MNGIE patients [9]. However, it does show some new functional and radiological alterations (neuromotor dysfunction and ventricular alterations in brain) that are absent or much less prominent in the non-nucleoside exposed murine model. We used this enhanced preclinical model to expand on our previous studies demonstrating the feasibility and efficacy of AAV-based liver-targeted gene therapy for MNGIE [19,21,23].

Systemic dThd and dUrd levels in naïve dKO mice were 2- to 4-fold higher than levels in naïve WT mice, as was originally reported [5] and consistently observed here, which contrasts with the much more pronounced accumulations (more than 50-fold) observed in MNGIE patients [35,36]. In agreement with the study where the stressed model was established [25], we found that oral administration of dThd and dUrd to dKO mice exacerbates systemic accumulation of both dNs. Furthermore, the highest dThd and dUrd accumulations were seen in small intestine, likely because of the presence of ingested dNs, before or during intestinal absorption. In contrast, we found detectable dThd and dUrd levels in all tissues analyzed from naïve WT mice, and exposed dKO mice had dN levels only 20-fold above WT plasma values, and 10-fold above liver and brain WT values. These discrepancies likely result from the use of TP activity inhibitors during sample processing for dN determination, which prevented in vitro dN degradation in WT samples and reduced the differences between naïve WT and exposed dKO concentrations. As was expected, the excess of dThd and dUrd resulted in enhanced mitochondrial dNTP imbalances (dTTP increase and dCTP depletion) in the two tissues analyzed (liver and brain).

We found an unreported effect of dN exposure on mice: an increase in TP activity in liver, but not in skeletal muscle, small intestine, or brain. A similar effect (*TYMP* upregulation) has been reported in cultured human cells in response to dThd and nucleoside analogues [37]. Exposure to dN doubled liver TP activity in WT mice and, interestingly, also increased activity in dKO animals. Upregulation of *Tymp* or other genes encoding enzymes with TP activity (such as *Upp1* and *Upp2*) may account for this increase in WT mice. Additionally, dThd excess could be inhibiting the ubiquitin-mediated TP degradation as it has been recently reported in human differentiating reticulocyte cell cultures [38]. In contrast, *Tymp* and *Upp1* genes are molecularly inactivated in the dKO model [5,39]; therefore, dN-induced TP activity in these animals should be mediated by upregulation of another enzyme, likely UP2 (encoded by *Upp2*). In fact, naïve dKO mice have some detectable TP activity in liver that must be due to UP2.

All MNGIE patients present diffuse leukoencephalopathy on brain MRI, but this abnormality is barely detectable in naïve dKO mice, and is only seen when they are very old [5]. The first study of the nucleoside-exposed dKO model demonstrated that chronic exposure to dThd and dUrd led to increased brain MRI FLAIR intensity signal around the third and lateral ventricles [25]. In our study, we failed to detect MRI differences between naïve dKO and naïve WT mice, showing how elusive this feature is in the unexposed mouse model. Nonetheless, and in agreement with the previous report [25], dKO mice (but not WT mice) did develop the MRI phenotype under dN exposure, although we found enlarged ventricle volumes rather than the diffuse parenchymal leukoencephalopathy that is typically observed in MNGIE patients. Combined analysis of T2 maps and high-resolution T2-weighted images revealed that the periventricular signal hyperintensity corresponds to enlarged ventricular volume, with no fluid transfer to the surrounding white matter, in contrast to what is observed in other hydrocephalic models with severe ventricular enlargement [40]. Exposure to dNs also succeeded in the development of a motor function phenotype. At 25 weeks of age, exposed dKO mice showed a shorter time to fall in the rotarod test, which is indicative of motor coordination impairment in this model, in agreement with previous findings [25]. Furthermore, rotarod time to fall at 25 weeks of age inversely correlated with MRI ventricular volume



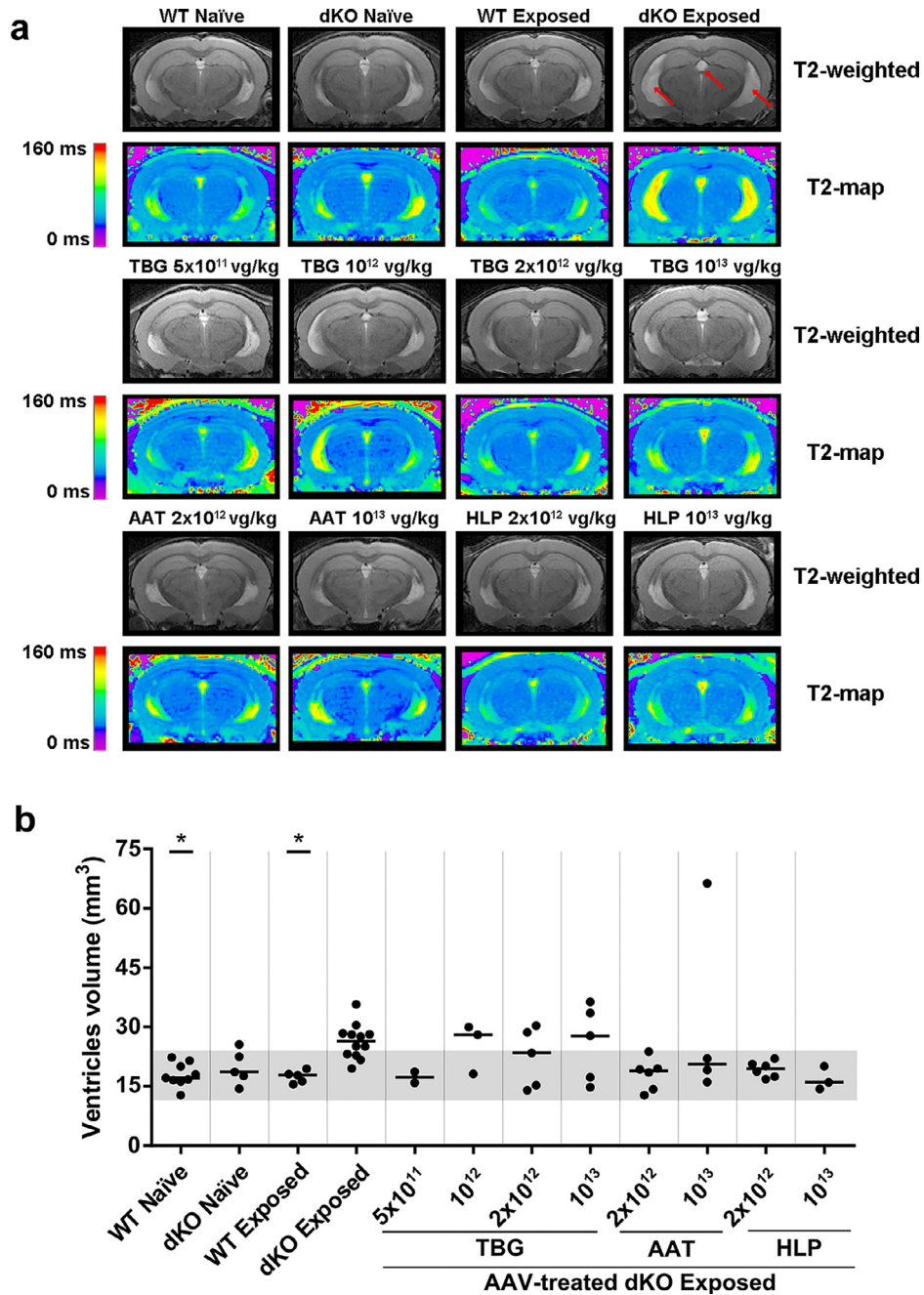


**Fig. 5.** Brain MRI analysis. (a) Coronal T2-weighted and T2 map images of 1-mm sections (region corresponding to slice 6 in Supp Figure S7) showing ventricular enlargement in dKO exposed mice (red arrows). (b) Ventricular volume in 80 to 84-weeks old WT ( $n = 9$ ) and dKO ( $n = 5$ ) naïve mice, non-treated WT ( $n = 5$ ) and dKO ( $n = 12$ ) exposed mice, and dKO exposed mice treated with different AAVs doses (TBG-treated mice with:  $5 \times 10^{11}$  vg/kg  $n = 2$ ,  $10^{12}$  vg/kg  $n = 3$ ,  $2 \times 10^{12}$  vg/kg  $n = 5$  and  $10^{13}$  vg/kg  $n = 5$ ; AAT-treated mice with:  $2 \times 10^{12}$  vg/kg  $n = 6$  and  $10^{13}$  vg/kg  $n = 4$ ; HLP-treated mice with:  $2 \times 10^{12}$  vg/kg  $n = 6$  and  $10^{13}$  vg/kg  $n = 3$ ). Ventricular volume was quantified in T2 maps as the sum of the ventricular volumes calculated in all sections analyzed in Supp Figure S6 (see materials and methods for calculations). Gray areas indicate the range of values in the naïve WT group. Asterisks indicate statistically significant differences ( $*p < 0.05$ ; Kruskal-Wallis test followed by the Dunn's multiple comparisons test, all groups compared with dKO exposed). Ventricular volume values above the mean plus 3 SD of all data were considered outliers and excluded from the analysis. Two outliers were identified in dKO exposed AAV-treated with TBG  $10^{12}$  vg/kg, and TBG  $2 \times 10^{12}$  vg/kg, one in each group.

assessed at 84 weeks of age, which concurs with previous studies associating hydrocephalus with motor function defects [41].

As was discussed above, most effects of dN exposure seen in our study are consistent with previously reported findings [25], but we failed to replicate some other important features. After careful histological analysis (Masson's trichrome staining), we found no abnormalities in small intestine of exposed mice, and no mtDNA depletion was detected in brain or in small intestine.

In previous preclinical studies, we used the TBG promoter in AAV gene therapy for MNGIE and proved that it is effective for driving

hcTYMP expression [21,23]. The need to optimize therapeutic gene expression and minimize the vector dose to transfer therapy to MNGIE patients prompted us to explore new vector constructs [19]. The ApoE-AAT enhancer-promoter cassette has been used in several AAV-based preclinical and clinical studies [42-45]. The self-complementary genome configuration resulted in faster and stronger therapeutic gene expression in these studies, and it has also been successfully used in patients [46-48]. We found that use of the AAV-AAT vector to carry hcTYMP in the dKO model resulted in greater efficacy as compared to other hepatic promoters or a self-

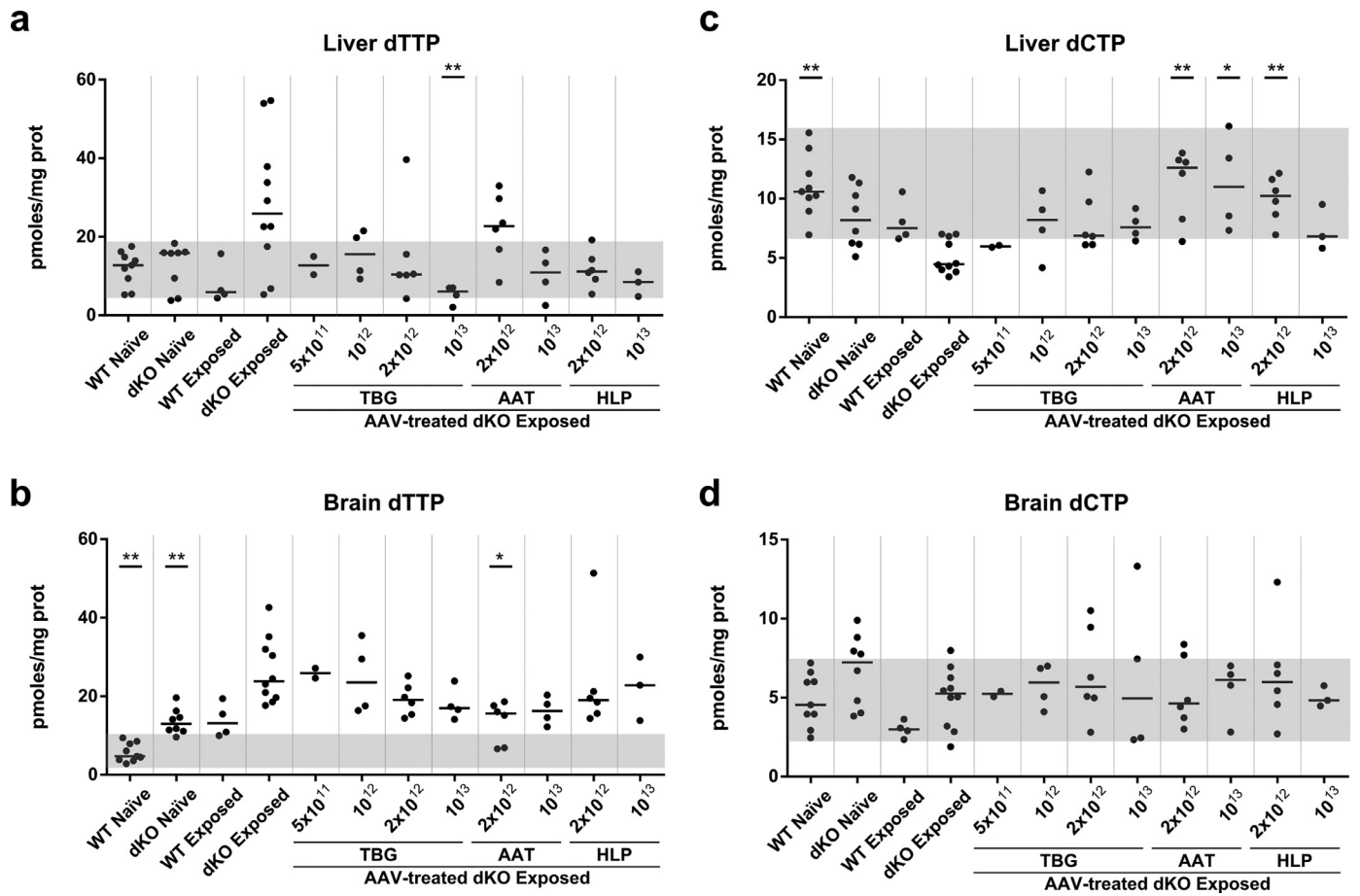


**Fig. 6.** Mitochondrial dNTPs. Mitochondrial thymidine triphosphate (dTTP) and deoxycytidine triphosphate (dCTP) content in liver (a and c) and brain (b and d) of WT ( $n = 9$ ) and dKO ( $n = 8$ ) naïve mice, non-treated WT ( $n = 4$ ) and dKO ( $n = 10$ ) exposed mice and dKO exposed mice treated with different AAVs doses (TBG-treated mice with:  $5 \times 10^{11}$  vg/kg  $n = 2$ ,  $10^{12}$  vg/kg  $n = 4$ ,  $2 \times 10^{12}$  vg/kg  $n = 6$  and  $10^{13}$  vg/kg  $n = 4$ ; AAT-treated mice with:  $2 \times 10^{12}$  vg/kg  $n = 6$  and  $10^{13}$  vg/kg  $n = 4$ ; HLP-treated mice with:  $2 \times 10^{12}$  vg/kg  $n = 6$  and  $10^{13}$  vg/kg  $n = 3$ ). Horizontal lines indicate the median for each group. Gray areas indicate the range of values in the naïve WT group. Asterisks indicate statistically significant differences ( $*p < 0.05$ ,  $**p < 0.01$ ; Kruskal-Wallis test followed by the Dunn's multiple comparisons test, all groups compared with dKO exposed).

complementary configuration [19]. Now, taking advantage of the enhanced nucleoside-exposed animal model to expand the study, we found that AAV-AAT provides an effect beyond the previously reported biochemical normalization. AAV-AAT performed better than other liver-targeted vectors in restoring biochemical homeostasis (nucleoside reduction, liver TP activity, dNTP normalization), and it also improved the brain MRI abnormalities manifested in the exposed mouse model.

Our attempts to determine the effect of different vectors on dN homeostasis revealed an unexpected limitation of the model. As mice received dNs in their drinking water ad libitum, the variability in dN levels seen over the day was likely determined by the last time the mouse drank water. To circumvent this confounding factor, we decided to determine PK parameters (peak concentration, AUC, and time to reach WT values) after a single gavage administration, instead of single dN values in one blood sample, as more reliable biochemical endpoints to study the effect of the vectors on dN homeostasis in the model. A vector dose-response was observed in most cases, and comparison between the three vectors showed that AAV-AAT was the most efficient to reduce plasma dN levels, which is consistent with their better comparative ability to provide TP activity to liver. As was expected, all vectors led to substantial dose-dependent TP activity in liver, and the analysis of TP activity/vector copy number ratios indicated that the AAT promoter was the most efficient. All these observations confirm and reinforce our previous results on the efficacy of different vectors [19].

Previously, we observed that treatment with AAV-TBG, AAV-HLP and AAV-AAT results in sporadic cases of increased TP activity in non-hepatic tissues [19], and this was confirmed here in an independent set of experiments. In our previous report, we found that this “illegitimate activity” seems not to be caused by ectopic expression, as transgene DNA or mRNA could not be consistently found in samples with TP activity. Hence, this activity might respond to exosomal export from liver [49]. In any case, this extra-hepatic effect was irrelevant in quantitative terms in both the previous and the current study.

dNTP imbalances were ameliorated in liver as a consequence of the systemic dN reduction. The effect in brain, however, was only partial. The fact that liver, but not brain, is the target of the vectors tested here may account for the modest effect in brain. In addition, the anatomic complexity of the brain, constituted by many cell types distributed among different functional areas, may mask local effects, as our method for mitochondrial dNTP determination is performed on total brain mitochondria. Interestingly, dCTP depletion could not be detected in brain mitochondria, which correlates with the absence of mtDNA depletion in this organ, in agreement with previous experimental data showing that the cause of mtDNA depletion in MNGIE is limited availability of dCTP [4].

Of note, this is the first time that AAV-mediated gene therapy has shown efficacy on disease-related features in MNGIE beyond normalization of the biochemical imbalances. Nucleoside-exposed mice treated with AAV-HLP and AAV-AAT vectors recovered normal

ventricular volumes on MRI, while this effect was only partial (in some mice) and not statistically significant with the AAV-TBG vector. When all mice were taken as a whole, ventricular volumes significantly correlated with dThd levels in brain, reinforcing the notion that normalization of the biochemical imbalances is directly related with improvements in this neurological trait. However, the results did not allow us to draw clear conclusions on the effect of therapy on motor function, as assessed with the rotarod test. Time to fall in the rotarod test was shorter in nucleoside-exposed dKO mice, which can be due to alterations in the central nervous system and/or the skeletal muscle. This reduction seemed to be prevented in most groups of AAV-treated mice. However, if this observation suggests a positive effect of the treatment, it is uncertain why was it not observed at the highest vector doses. The reasons for this apparent paradox remain to be explored.

The results of this study show that the AAV-AAT vector performed the best among those tested, efficiently providing TP activity to the liver and restoring dN and dNTP homeostasis. In addition, functional improvements on the phenotype beyond normalization of biochemical markers were proven for AAV-mediated MNGIE gene therapy in the nucleoside-exposed dKO mouse model. AAV transduction rates are lower in humans than in mice [50,51]; therefore, using more potent promoters, within a reasonable range of potency, will be necessary to make AAV treatment possible in humans at feasible vector doses. This will have an impact on both biosafety and the cost of treatment, and contribute to facilitating implementation of this therapy in patients, which constitutes a significant advance towards the treatment of this devastating disorder with a much less invasive therapy than those currently available.

## Contributors

F. Vila-Julà, J. Torres-Torronteras and R. Martí designed the study and wrote the manuscript; F. Vila-Julà, R. Cabrera-Pérez, Y. Cámara, M. Molina-Berenguer, S. Lope-Piedrafita, and J. Torres-Torronteras performed the experiments and collected and analysed the data; F. Vila-Julà, S. Lope-Piedrafita, J. Torres-Torronteras and R. Martí participated in data interpretation; M. Hirano generated and provided the mouse model; F. Mingozzi produced and provided the AAV-AAT vector; all the participating authors contributed to the critical revision of the manuscript. All the authors read and approved the final version of the manuscript.

## Declaration of Competing Interests

RM, FV and MM report grants from the *Instituto de Salud Carlos III* during the conduct of the study; JT reports grants from Departament de Salut, Generalitat de Catalunya (PERIS program), during the conduct of the study; RM, MH, JT and YC report grants and non-financial support from Modis Therapeutics, personal fees and other from Modis Therapeutics, outside the submitted work; in addition, RM and MH have a patent “Deoxynucleoside therapy for diseases caused by unbalanced nucleotide pools including mitochondrial DNA depletion syndromes” (PCT/US16/038110) with royalties paid to Modis Therapeutics; MH reports grants and other support from Entrada Therapeutics, grants from Muscular Dystrophy Association and grants from NIH, outside the submitted work; FM is an employee of Spark Therapeutics; SL reports that the Nuclear Magnetic Resonance facility where she works charged the VHIR a fee for the MRI services; and RM, YC, JT and RC have a patent “Treatment of mitochondrial diseases” (PCT/EP2016/062636) with royalties paid to Modis Therapeutics.

## Acknowledgments

JT and FV were funded by fellowships granted by the Generalitat de Catalunya (PERIS program, [SLT002/16/00370](#) to JT and [FI-AGAU](#)

program [2018FL\\_B\\_01115](#) to FV). This work was funded in part by the Spanish Instituto de Salud Carlos III (Grants [PI15/00465](#), [PMP15/00025](#) and [PI18/01574](#) to R.M., co-funded with E.R.D.F.). The disclosed funders had no role in study design, data collection and analysis, decision to publish, or preparation of the manuscript.

## Data sharing statement

The data that support the findings of this study are available from the corresponding authors, RM and JT, upon reasonable request.

## Supplementary materials

Supplementary material associated with this article can be found, in the online version, at [doi:10.1016/j.ebiom.2020.103133](https://doi.org/10.1016/j.ebiom.2020.103133).

## References

- [1] Nishino I, Spinazzola A, Hirano M. Thymidine phosphorylase gene mutations in MNGIE, a human mitochondrial disorder. *Science* 1999;283(5402):689–92.
- [2] Martí R, Nishigaki Y, Hirano M. Elevated plasma deoxyuridine in patients with thymidine phosphorylase deficiency. *Biochem Biophys Res Commun* 2003;303(1):14–8.
- [3] Spinazzola A, Martí R, Nishino I, Andreu AL, Naini A, Tadesse S, et al. Altered thymidine metabolism due to defects of thymidine phosphorylase. *J Biol Chem* 2002;277(6):4128–33.
- [4] Gonzalez-Vioque E, Torres-Torronteras J, Andreu AL, Martí R. Limited dCTP availability accounts for mitochondrial DNA depletion in mitochondrial neurogastrointestinal encephalomyopathy (MNGIE). *PLoS Genet* 2011;7(3):e1002035.
- [5] Lopez LC, Akman HO, Garcia-Cazorla A, Dorado B, Martí R, Nishino I, et al. Unbalanced deoxynucleotide pools cause mitochondrial DNA instability in thymidine phosphorylase-deficient mice. *Hum Mol Genet* 2009;18(4):714–22.
- [6] Nishigaki Y, Martí R, Copeland WC, Hirano M. Site-specific somatic mitochondrial DNA point mutations in patients with thymidine phosphorylase deficiency. *J Clin Invest* 2003;111(12):1913–21.
- [7] Nishigaki Y, Martí R, Hirano M. ND5 is a hot-spot for multiple atypical mitochondrial DNA deletions in mitochondrial neurogastrointestinal encephalomyopathy. *Hum Mol Genet* 2004;13(1):91–101.
- [8] Pontarin G, Ferraro P, Valentino ML, Hirano M, Reichard P, Bianchi V. Mitochondrial DNA depletion and thymidine phosphate pool dynamics in a cellular model of mitochondrial neurogastrointestinal encephalomyopathy. *J Biol Chem* 2006;281(32):22720–8.
- [9] Garone C, Tadesse S, Hirano M. Clinical and genetic spectrum of mitochondrial neurogastrointestinal encephalomyopathy. *Brain* 2011;134(Pt 11):3326–32.
- [10] Cabrera-Pérez R, Torres-Torronteras J, Vila-Julà F, Ortega FJ, Cámara Y, Barquero J, et al. Prospective therapeutic approaches in mitochondrial neurogastrointestinal encephalomyopathy (MNGIE). *Expert Opin Orphan Drugs* 2015;3(10):1167–82.
- [11] Halter J, Schupbach WM, Casali C, Elhasid R, Fay K, Hammans S, et al. Allogeneic hematopoietic SCT as treatment option for patients with mitochondrial neurogastrointestinal encephalomyopathy (MNGIE): a consensus conference proposal for a standardized approach. *Bone Marrow Transpl* 2010;46(3):330–7.
- [12] Hirano M, Martí R, Casali C, Tadesse S, Uldrick T, Fine B, et al. Allogeneic stem cell transplantation corrects biochemical derangements in MNGIE. *Neurology* 2006;67(8):1458–60.
- [13] Halter JP, Michael W, Schupbach M, Mandel H, Casali C, Orchard K, et al. Allogeneic haematopoietic stem cell transplantation for mitochondrial neurogastrointestinal encephalomyopathy. *Brain* 2015;138(Pt 10):2847–58.
- [14] Boschetti E, D'Alessandro R, Bianco F, Carelli V, Cenacchi G, Pinna AD, et al. Liver as a source for thymidine phosphorylase replacement in mitochondrial neurogastrointestinal encephalomyopathy. *PLoS ONE* 2014;9(5):e96692.
- [15] D'Angelo R, Boschetti E, Amore G, Costa R, Pugliese A, Caporali L, et al. Liver transplantation in mitochondrial neurogastrointestinal encephalomyopathy (MNGIE): clinical long-term follow-up and pathogenic implications. *J Neurol* 2020.
- [16] D'Angelo R, Rinaldi R, Pironi L, Dotti MT, Pinna AD, Boschetti E, et al. Liver transplant reverses biochemical imbalance in mitochondrial neurogastrointestinal encephalomyopathy. *Mitochondrion* 2017;34:101–2.
- [17] De Giorgio R, Pironi L, Rinaldi R, Boschetti E, Caporali L, Capristo M, et al. Liver transplantation for mitochondrial neurogastrointestinal encephalomyopathy. *Ann Neurol* 2016;80(3):448–55.
- [18] Kripps K, Nakayuenyongsuk W, Shayota BJ, Berquist W, Gomez-Ospina N, Esquivel CO, et al. Successful liver transplantation in mitochondrial neurogastrointestinal encephalomyopathy (MNGIE). *Mol Genet Metab* 2020;130(1):58–64.
- [19] Cabrera-Pérez R, Vila-Julà F, Hirano M, Mingozzi F, Torres-Torronteras J, Martí R. Alpha-1-antitrypsin promoter improves the efficacy of an adeno-associated virus vector for the treatment of mitochondrial neurogastrointestinal encephalomyopathy. *Hum Gene Ther* 2019;30(8):985–98.
- [20] Torres-Torronteras J, Cabrera-Pérez R, Barba I, Costa C, de Luna N, Andreu AL, et al. Long-term restoration of thymidine phosphorylase function and nucleoside

- homeostasis using hematopoietic gene therapy in a murine model of mitochondrial neurogastrointestinal encephalomyopathy. *Hum Gene Ther* 2016;27(9):656–67.
- [21] Torres-Torronteras J, Cabrera-Pérez R, Vila-Julià F, Viscomi C, Cámara Y, Hirano M, et al. Long-term sustained effect of liver-targeted adeno-associated virus gene therapy for mitochondrial neurogastrointestinal encephalomyopathy. *Hum Gene Ther* 2018;29(6):708–18.
- [22] Torres-Torronteras J, Gomez A, Eixarch H, Palenzuela L, Pizzorno G, Hirano M, et al. Hematopoietic gene therapy restores thymidine phosphorylase activity in a cell culture and a murine model of MNGIE. *Gene Ther* 2011;18(8):795–806.
- [23] Torres-Torronteras J, Viscomi C, Cabrera-Perez R, Camara Y, Di Meo I, Barquinerio J, et al. Gene therapy using a liver-targeted AAV vector restores nucleoside and nucleotide homeostasis in a murine model of MNGIE. *Mol Ther* 2014;22(5):901–7.
- [24] Yadak R, Cabrera-Pérez R, Torres-Torronteras J, Bugiani M, Haecck JC, Huston MW, et al. Preclinical efficacy and safety evaluation of hematopoietic stem cell gene therapy in a mouse model of MNGIE. *Mol Ther Methods Clin Dev* 2018;8:152–65.
- [25] Garcia-Diaz B, Garone C, Barca E, Mojahed H, Gutierrez P, Pizzorno G, et al. Deoxy-nucleoside stress exacerbates the phenotype of a mouse model of mitochondrial neurogastrointestinal encephalopathy. *Brain* 2014;137(Pt 5):1337–49.
- [26] McIntosh J, Lenting PJ, Rosales C, Lee D, Rabbanian S, Raj D, et al. Therapeutic levels of FVIII following a single peripheral vein administration of rAAV vector encoding a novel human factor VIII variant. *Blood* 2013;121(17):3335–44.
- [27] Davidoff AM, Ng CY, Zhou J, Spence Y, Nathwani AC. Sex significantly influences transduction of murine liver by recombinant adeno-associated viral vectors through an androgen-dependent pathway. *Blood* 2003;102(2):480–8.
- [28] Bradford MM. A rapid and sensitive method for the quantitation of microgram quantities of protein utilizing the principle of protein-dye binding. *Anal Biochem* 1976;72:248–54.
- [29] Martí R, López LC, Hirano M. Assessment of thymidine phosphorylase function: measurement of plasma thymidine (and deoxyuridine) and thymidine phosphorylase activity. *Methods Mol Biol* (Clifton, NJ) 2012;837:121–33.
- [30] Pérez-Pérez MJ, Priego EM, Hernández AI, Camarasa MJ, Balzarini J, Liekens S. Thymidine phosphorylase inhibitors: recent developments and potential therapeutic applications. *Mini Rev Med Chem* 2005;5(12):1113–23.
- [31] Sherman PA, Fyfe JA. Enzymatic assay for deoxyribonucleoside triphosphates using synthetic oligonucleotides as template primers. *Anal Biochem* 1989;180(2):222–6.
- [32] Blázquez-Bermejo C, Molina-Granada D, Vila-Julià F, Jiménez-Heis D, Zhou X, Torres-Torronteras J, et al. Age-related metabolic changes limit efficacy of deoxy-nucleoside-based therapy in thymidine kinase 2-deficient mice. *EBioMedicine* 2019;46:342–55.
- [33] Moolenbeek C, Ruitenbergh EJ. The "Swiss roll": a simple technique for histological studies of the rodent intestine. *Lab. Anim.* 1981;15(1):57–9.
- [34] Hirano M, Casali C, Tadesse S, Stanzani M, Savage D. Sustained biochemical and clinical improvements two years postallogeic stem cell transplantation in a patient with MNGIE. *Neurology* 2008;70:A406–A7.
- [35] Marti R, Spinazzola A, Tadesse S, Nishino I, Nishigaki Y, Hirano M. Definitive diagnosis of mitochondrial neurogastrointestinal encephalomyopathy by biochemical assays. *Clin Chem* 2004;50(1):120–4.
- [36] Valentino ML, Marti R, Tadesse S, Lopez LC, Manes JL, Lyzak J, et al. Thymidine and deoxyuridine accumulate in tissues of patients with mitochondrial neurogastrointestinal encephalomyopathy (MNGIE). *FEBS Lett* 2007;581(18):3410–4.
- [37] Tsuneyoshi K, Haraguchi M, Hongye Z, Gotanda T, Tachiwada T, Sumizawa T, et al. Induction of thymidine phosphorylase expression by AZT contributes to enhancement of 5'-DFUR cytotoxicity. *Cancer Lett* 2006;244(2):239–46.
- [38] Meinders M, Shoemark D, Dobbe JGG, Streekstra GJ, Frayne J, Toye AM. Expression and retention of thymidine phosphorylase in cultured reticulocytes as a novel treatment for MNGIE. *Mol Ther Methods Clin Dev* 2020;17:822–30.
- [39] Cao D, Leffert JJ, McCabe J, Kim B, Pizzorno G. Abnormalities in uridine homeostatic regulation and pyrimidine nucleotide metabolism as a consequence of the deletion of the uridine phosphorylase gene. *J Biol Chem* 2005;280(22):21169–75.
- [40] Mandell JG, Neuberger T, Drapaca CS, Webb AG, Schiff SJ. The dynamics of brain and cerebrospinal fluid growth in normal versus hydrocephalic mice. *J Neurosurg Pediatr* 2010;6(1):1–10.
- [41] Lee MJ, Chang CP, Lee YH, Wu YC, Tseng HW, Tung YY, et al. Longitudinal evaluation of an N-ethyl-N-nitrosourea-created murine model with normal pressure hydrocephalus. *PLoS ONE* 2009;4(11):e7868.
- [42] George LA, Sullivan SK, Giermasz A, Rasko JEJ, Samelson-Jones BJ, Ducore J, et al. Hemophilia B gene therapy with a high-specific-activity factor IX variant. *N Engl J Med* 2017;377(23):2215–27.
- [43] Manno CS, Pierce GF, Arruda VR, Glader B, Ragni M, Rasko JJ, et al. Successful transduction of liver in hemophilia by AAV-Factor IX and limitations imposed by the host immune response. *Nat Med* 2006;12(3):342–7.
- [44] Miao CH, Ohashi K, Patijn GA, Meuse L, Ye X, Thompson AR, et al. Inclusion of the hepatic locus control region, an intron, and untranslated region increases and stabilizes hepatic factor IX gene expression in vivo but not in vitro. *Mol Ther* 2000;1(6):522–32.
- [45] Nayak S, Herzog RW. Progress and prospects: immune responses to viral vectors. *Gene Ther* 2010;17(3):295–304.
- [46] Nathwani AC, Gray JT, Ng CY, Zhou J, Spence Y, Waddington SN, et al. Self-complementary adeno-associated virus vectors containing a novel liver-specific human factor IX expression cassette enable highly efficient transduction of murine and nonhuman primate liver. *Blood* 2006;107(7):2653–61.
- [47] Nathwani AC, Reiss UM, Tuddenham EG, Rosales C, Chowdary P, McIntosh J, et al. Long-term safety and efficacy of factor IX gene therapy in hemophilia B. *N Engl J Med* 2014;371(21):1994–2004.
- [48] Wang Z, Ma HI, Li J, Sun L, Zhang J, Xiao X. Rapid and highly efficient transduction by double-stranded adeno-associated virus vectors in vitro and in vivo. *Gene Ther* 2003;10(26):2105–11.
- [49] Simpson RJ, Kalra H, Mathivanan S. ExoCarta as a resource for exosomal research. *J Extracell Vesicles* 2012;1.
- [50] Lisowski L, Dane AP, Chu K, Zhang Y, Cunningham SC, Wilson EM, et al. Selection and evaluation of clinically relevant AAV variants in a xenograft liver model. *Nature* 2014;506(7488):382–6.
- [51] Vercauteren K, Hoffman BE, Zolotukhin I, Keeler GD, Xiao JW, Basner-Tschakarjan E, et al. Superior in vivo transduction of human hepatocytes using engineered AAV3 capsid. *Mol Ther* 2016;24(6):1042–9.